High Temperatures-High Pressures, Vol. 51, pp. 89–108
Reprints available directly from the publisher
Photocopying permitted by license only
DOI: 10.32908/hthp.v51.1003

Thermo-mechanical characterization of carbon-based ceramic foams for high temperature space application

Marta Albano[1], Aleksey V. Nenarokomov[2,*], Roberto Pastore[3], Sergey A. Budnik[2], Andrea Delfini[4], Oleg M. Alifanov[2], Mario Marchetti[3], Alena V. Morzhukhina[2], Dmitry M. Titov[2], Fabio Santoni[3], Fabrizio Piergentili[4] and Andrey V. Netelev[2]

[1]*Agenzia Spaziale Italiana, via del Politecnico snc, 00133 Rome, Italy*
[2]*Department of Space Systems Engineering, Moscow Aviation Institute, Volokolamskoe Hgw. 4, 125993, Moscow, Russia*
[3]*Department of Astronautic, Electric and Energetic Engineering, Sapienza University of Rome, via Eudossiana 18, 00184, Rome, Italy*
[4]*Department of Mechanical and Aerospace Engineering, Sapienza University of Rome, via Eudossiana 18, 00184, Rome, Italy*

Received: June 24, 2021; Accepted: September 21, 2023.

The successful development of aerospace reusable launch vehicles (RLV) require to realize effective thermal protection systems (TPS) for preserving spacecraft integrity from the severe thermal loads during re-entry phase. To such an aim, due to the need of reducing payload transportation costs, applied research is driven towards lightweight materials with advanced thermo-mechanical properties. Space TPS are often based on sandwich structures, where the core material has the main function of thermal insulation. Ceramic porous materials, as carbon (C) and silicon carbide (SiC) foams, represent ideal candidates for application as structural TPS component, thanks to both low density and significant thermal stability at very high temperatures. The paper presents a joint experimental study of carbon-based ceramic foams proposed as sandwich's core for TPS design. A full thermal characterization of commercial C- and SiC-foam materials is reported, including measurements of thermo-mechanical combined stress, temperature-induced outgassing behavior and heat transfer properties. These latter, in particular, are studied by means of a

*Corresponding author: aleksey.nenarokomov@mai.ru

robust numerical technique, known as the inverse method, which allows to evaluate materials thermal conductivity and heat capacity over a wide range of temperatures, thus establishing the required material behavior for potential use in spacecraft TPS.

Keywords: carbon foam, SiC foam, thermal protection, inverse problems

1 INTRODUCTION

The development of reusable launch vehicle (RLV) must include a significant reduction of the payload transportation costs. One of the most expensive part for any RLV is the thermal protection system (TPS), which has the function of protecting the vehicle from the high thermal loads during re-entry phase [1–4]. Thermal protection systems are typically constituted by sandwich structures (i.e., inner 'core' panels enclosed by upper/lower 'skin' layers) metallic or ceramic, which are required to be reusable, lightweight and thin [5–7]. Nowadays, systems and sub-systems multi-functionality is required in spacecraft design due to the several environmental threats; beside the specific capability, a system should thus behave also as structural part, resist to multiple loads, act as electromagnetic shield, etc. [8]. In this perspective, in order to perform satisfactorily, the TPS sandwich construction shall consider a core having effective mechanical performances, thermal characteristics and dielectric properties under conditions of use and still conform to weight limitations. In particular, for space and hypersonic vehicles applications the core material should withstand high thermal loads, the main task being to put down temperatures of hundreds of degree at the upper surface (typically about 1000–1500°C) in order to protect the inner volume of the spacecraft.

Many are the core typologies, from honeycombs to corrugated card/fiberboards, up to ceramic foam materials. About these latter, manufacturing methods are elaborated in order to achieve stable and multiple properties such as impressive stiffness, thermo-chemical durability, and electromagnetic compatibility [9–12]. In fact, such macro-cellular components attracted great attention due to unique properties as low density and thermal conductivity, high fluid permeability, thermal shock resistance and chemical stability as well as specific strength. For these reasons, ceramic foams are largely used in space transportation systems: usual applications are in launchers external tanks, re-entry vehicles, sample return missions, etc. As insulator in thermal protection systems, the key features of the foams are the low volume fraction of the solid phase which limits the conduction, the small cell size which virtually eliminates convection and reduces radiation through repeated absorption/reflection at the cell walls and the poor conductivity of the enclosed gas (or vacuum). An additional advantage is an excellent thermal shock resistance due to relatively low modulus compared to the bulk material. The foam selection is especially crucial as far as the sandwich's core optimization is

concerned, since failures of sandwich panels occur usually in the core because foams have low shear rigidity compared to the skins.

In space high temperature applications and in particular when the design implements ceramic matrix composites, one of the most efficient solution is to use carbon-based foams due to chemical compatibility and to lower levels of induced mechanical loads. These materials consist of solid carbonic struts arranged in space to form polyhedral cellular voids: they can be made with a multitude of processes, since the several available precursors as thermosetting, thermoplastic and hydrocarbon vapors [13–15]. The major categories are reticulated vitreous carbon foam, graphitic and non-graphitic carbon foam: in particular, the foams fabricated from thermosetting resin pyrolysis are reticulated vitreous carbon (RVC) network composed of glass-like carbon with high void volume, low density and rigid structure, high resistance to combustion, good electrical conductivity and microwave absorption properties [12, 16, 17]. Higher density foams, sometimes formulated with phenolic resins, provide further dimensional stability at elevated temperatures. For example, SiC foams are basically carbon foams which are infiltrated by means of chemical (silicide-)vapor deposition (CVD) method: such stable and proven manufacturing process guarantees a higher reliability with respect to other materials which can be considered as semi-finished products [10, 18, 19].

This work is a part of a large experimental study dealing with the physical properties of model RVC foams as function of their porous structures. Two commercial C- and SiC-foams were thoroughly investigated in terms of thermo-mechanical and heat transport properties, in order to assess the basic insulating capabilities provided by such materials when adopted as TPS core. To validate foams in sight of reliable space applications, a number of specimens were further subjected to compression test as the most usual type of loading for such kind of brittle material within a sandwich-like structure, as well as to outgassing characterization in order to analyze the compliance to thermal cycling/ultra-high vacuum conditions of space environment.

2 MATERIALS AND METHODS

2.1 Carbon and Silicon carbide foam

Two kind of commercial C- and SiC-foam materials were considered in this work, Goodfellow RVC foam and Panel SiC Ultramet (Touchstone Reasearch Laboraotory), respectively. As well known, properties and performances of cellular ceramics are strongly dependent on porosity (i.e., pores' size, distribution, interconnection and orientation) as well as on materials type and surface morphology. The micrographs reported in Fig. 1 show the bulk 3-D structure of the two typologies of foam analyzed, highlighting the more compact composition of SiC lattice respect to what occurs in only-C material.

Porosity defines how finely the foam raw material is arranged and interacts with the surrounding environment; thus, while the structural shape can be considered similar, a low pore-per-inch (PPI) foam will appear more hollow than higher PPI foams, such difference affecting crucial properties as specific surface area and fluid flow resistance. The nominal PPI value of the foams, as well as an approximate estimation of both average pore size as inferred by microscope inspection and of apparent density as measured by buoyancy method are reported in the figure caption.

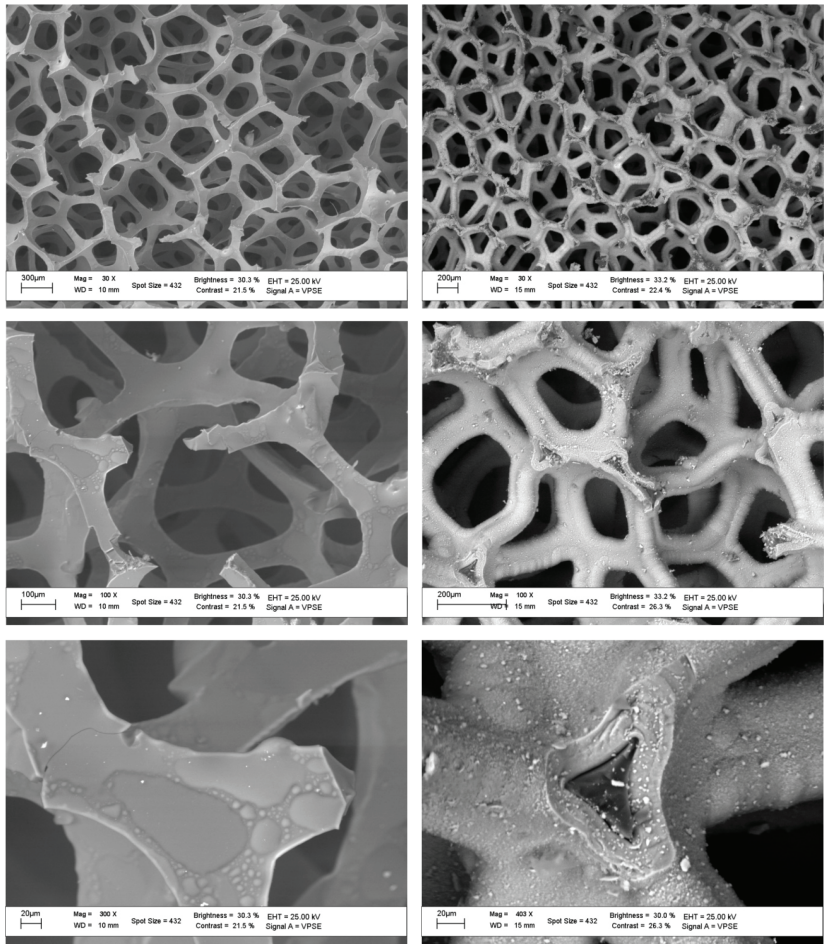

FIGURE 1
SEM images of C-foam (left) and SiC-foam (right) samples at growing magnifications – parameters [12]:

C-foam: PPI ~60, av. pore size ~400 µm, density ~0.05 g/cm^3.
SiC-foam: PPI ~45, av. pore size ~200 µm, density ~0.50 g/cm^3.

2.2 Thermal characterization

A preliminary analysis of the thermal behavior of the materials under test was carried out by measurements of the linear coefficient of thermal expansion (CTE), performed by a dedicate facility according to ASTM E228D standard. A horizontal dilatometer L75HX1600 facility was used, equipped by an outer tube which constitutes the thermal conditioning chamber, including the sample housing and a pushrod. The temperature range of the facility is RT-1600°C; the measuring head, connected to the pushrod, records the sample linear expansion which is used for data processing and CTE evaluation. Pictures of the set-up configuration and of a foam sample before the test are given in Fig. 2. The adopted facility is particularly suite for a complete validation of materials to be employed within the harsh thermal conditions of space environment: with respect to conventional optical sensor-based devices, in fact, the developed experimental set-up is able to reproduce the thermo-mechanical stress suffered by a component integrated within the whole spacecraft structure, thus giving a more reliable hint about the material effective behavior during thermal cycles or after sharp temperature raising [20, 21].

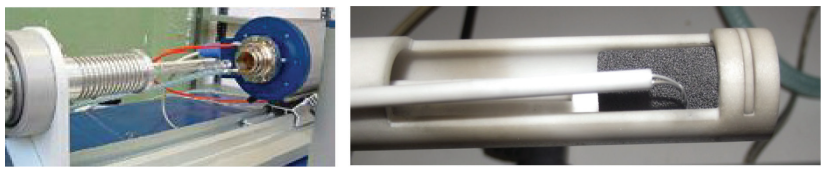

FIGURE 2
CTE measurements: horizontal dilatometer in open configuration (left), housing of a SiC foam test sample near the pushrod (right).

2.3 Mechanical test

About the evaluation of the materials mechanical properties, the tensile behavior was considered as the most critical for the proposed structural design, since compression loads represent the principal source of mechanical stress for a sandwich core. Tensile tests were performed using a Schenck Trebel Tester, following ASTM C365 standard: the testing machine is equipped with U2B/class-00 20kN load cell and a METIOR TRZ200 2kN load cell, both with nominal sensitivity of 2mV/V. The test is performed using the constant rate of transverse mode (see Fig. 3); the clamps used are compliant with the reference standard and are chosen in order to guarantee the right load alignment during the compressive phase.

2.4 Outgassing behavior

The outgassing test facility (OTF) at Aerospace System Laboratory (LSA – DIAEE of Sapienza University of Rome) allows to perform space materials tests in compliance with ASTM E-595 standard [22]. The test determines the

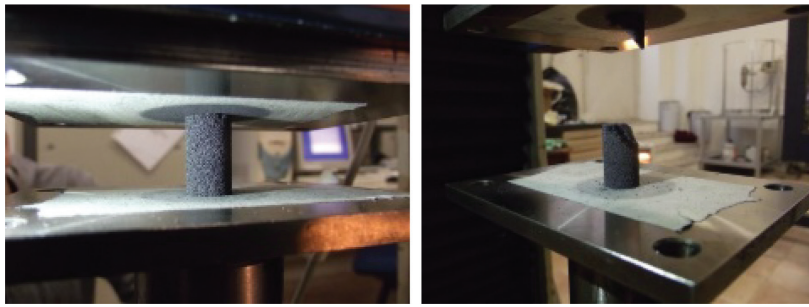

FIGURE 3
Compression break-load measurements: SiC foam sample during (left) and after (right) a tensile test.

volatile content of materials when exposed to vacuum environment (pressure down to 10^{-5} mbar) at relatively high temperature (up to 125°C). The outgassing behavior is evaluated by measurements of weight – i.e., of the mass loss by vaporization from the specimen's surface and of the amount of matter re-condensed on a 'cold' collector (kept at 25°C); the weights are measured by means of a Mettler-Toledo XP26DR balance (sensitivity 2 μg). Comparing to the weights measured before the test, 'total mass loss' (TML) and 'collected volatile condensable materials' (CVCM) are expressed as percentages of the initial specimen mass; two more parameters may be evaluated after a further conditioning step, the as called 'regained mass loss' (RML) represents the percentage of effective mass loss by outgassing taking into account the weight recovered due to moisture sorption, while the 'water vapor regained' (WVR) is the relative amount of vapor re-absorbed by the sample (see parameters definition in Tab. 1 legend). The criteria usually adopted for materials acceptance are determined by the end-user and based upon specific component and system requirements in terms of outgassing parameter thresholds: conventionally, TML of 1.00% and CVCM of 0.10% are indicated as screening levels for rejection of spacecraft materials, though the restriction may be less or even more stringent depending on the structures assembly/functionality as well as on the mission itself peculiarity.

2.5 Heat transfer analysis

The determination of heat transport properties as thermal conductivity and heat capacity was addressed by an experimental-computational method based on the inverse problems of heat transfer (IPHT) technique. An advanced hardware developed at Moscow Aviation Institute (MAI – Department of Space Systems Engineering) was devised to provide materials thermal conditioning and heat conduction monitoring. The laboratory set-up includes a high-temperature thermo-vacuum stand TVS-2M, special experimental modules (EM-3D) for realization of heat transfer models in the testing of specimens,

an automated system (AS) of heating control, experimental information measurements, collection and processing based on PC/PXI modules, hardware of local network providing interconnection of the system with distant workbenches, and a special technological equipment for the preparation of experimental specimens including the manufacture of thermo-sensors to be installed within the material under test. The experimental set-up was exploited by using symmetric heating, which ensures a reliable estimation of heat flux from the heater. The two specimens of carbon foam and two specimens of SiC foam (100ppi) were tested using symmetrical heating approach (Fig. 4).

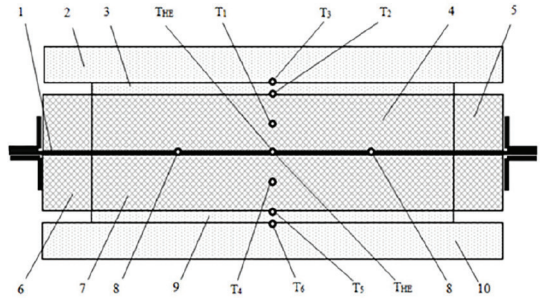

FIGURE 4
A testing scheme for specimens.
1 – heating element (HE), 2 – upper insulator, 3 – heat flux sensor on the specimen A, 4 – SiC experimental specimen A (upper), 5 – insulator of specimen A, 6 – insulator of specimen B, 7 – SiC experimental specimen B, 8 – points of voltage measurement on HE, 9 – heat flux sensor on the specimen B, 10 – lower insulator. Thermocouples: THE – control thermocouple on HE; T1 – internal in specimen A, T2 – on the heating surface of heat flux sensor of specimen A, T3 – on the back surface of heat flux sensor of specimen A, T4 – internal in specimen A, T5 – on the heating surface of heat flux sensor of specimen B, T6 – on the back surface of heat flux sensor of spacemen B.

The elements 2 and 10, and heat flux sensors were manufactured from insulating materials with thermal stability till 1500K (SiC fibers). The elements 5 and 6 was manufactured from insulating materials with thermal stability till 2000K (Al_2O_3 fibers). The thickness of Tantalum HE was 0.1 mm. The tests of SiC material were carried out in vacuum with pressure $1 \times 10^{-7} \div 1 \times 10^{-6}$ bar. Full details about the used equipment can be found in [23, 24].

Heat flux from HE can be estimated as:

$$q_{HE}(\tau) = \frac{N}{2 \cdot S} - \frac{\rho_{HE} \delta_{HE} C_{HE}}{2} \cdot \frac{dT_{HE}}{d\tau},$$

where heat capacity can be estimated as $C(T) = 135,77 + 0,0242 \times T$, and S is 0,0036135 m^2.

Pictures of as received SiC foam slices and of the same specimens after the high temperature (up to 1700°C) test are given in Fig. 5. The mass loses in the testing were for specimen A ~ 1,5% and for specimen B ~ 2,6%.

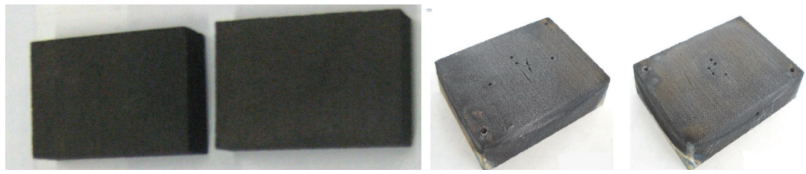

FIGURE 5
SiC foam samples before (left) and after (right) high temperature heat transport test.

It is assumed that heat transfer in carbon and SiC foams can be considered as a heat conduction with the effective thermal conductivity coefficient. Of course this approach is not applicable near the heating boundaries of the foam layer, because thermal radiation in an absorbing and scattering foam is the main mode of heat transfer for high temperature, but in the test heating surface was covered by special high temperature coating [24]. The experimental work presented in this paper does not pretend to a detailed physically analysis. A general physical analysis of heat transfer in highly porous materials should be based on the spectral analysis of the radiative transfer problem and can be found at [25–32].

Based on the given set-up configuration, a mathematical modeling of heat transfer across the material's specimen (infinite two-layer slab of known thickness) can be presented as follows, introducing the volumetric heat capacity (C) and conductivity (λ) as function of temperature (T), time (τ) and position (x):

$$C_l(T)\frac{\partial T_l}{\partial \tau}=\frac{\partial}{\partial x}\left(\lambda_l(T)\frac{\partial T_l}{\partial x}\right)\quad X_{l-1}<x<X_l, l=\overline{1,2},\quad 0\le\tau\le\tau_{\max} \tag{1}$$

$$T_1(x,0)=T_1^0(x),\ X_{l-1}<x<X_l,\ l=\overline{1,2} \tag{2}$$

$$-\lambda_1(T)\frac{\partial T_1(X_0,\tau)}{\partial x}=q_1(\tau),\quad \tau\in(\tau_{\min},\tau_{\max}] \tag{3}$$

$$\lambda_1(T_1(X_1,\tau))\frac{\partial T_1(X_1,\tau)}{\partial x}=\lambda_2(T_2(X_1,\tau))\frac{\partial T_2(X_1,\tau)}{\partial x} \tag{4}$$

$$T_1(X_1,\tau)=T_2(X_1,\tau) \tag{5}$$

$$-\lambda(T)\frac{\partial T(X_1,\tau)}{\partial x}=q_2(\tau),\quad \tau\in(\tau_{\min},\tau_{\max}] \tag{6}$$

In models (1)–(6) the coefficients $C_1(T)$ and $\lambda_1(T)$ are unknown.

The complimentary information needed for solving the inverse problem prescribed are the results of the temperature measurements

$$T^{\exp}(X_m,\tau)=f_m(\tau),\quad m=\overline{0,2}, \tag{7}$$

Let us introduce in the interval $[T_{\min},T_{\max}]$ two uniform difference grids *i*th the number of nodes N_i, $i = 1, 2$, namely

$$\omega_i=\left\{T_k=T_{\min}+(k-1)\Delta T,\ k=\overline{1,N_i}\right\},\quad i=\overline{1,2} \tag{8}$$

We approximate the unknown functions on grids (6) using cubic B-splines as follows

$$C_1(T)=\sum_{k=1}^{N_1}C_k\phi_k^1(T),\qquad \lambda_1(T)=\sum_{k=1}^{N_2}\lambda_k\phi_k^2(T), \tag{9}$$

where C_k, $k=\overline{1,N_1}$, λ_k, $k=\overline{1,N_2}$, are parameters. A_s a result of the approximation, the inverse problem is reduced to a search for the vector of unknown parameters $\overline{p}=\{p_k\},k=\overline{1,N_p}$, which has dimension $N_p=N_1+N_2$.

The least-square residual of computational and measured temperatures at points of the thermocouple installation is given by:

$$J(C_1(T),\lambda_1(T))=\sum_{m=0}^{2}\int_{\tau_{\min}}^{\tau_{\max}}(T(X_m,\tau)-f_m(\tau))^2\,d\tau\,, \tag{10}$$

where $T(x_m,\tau)$ is defined from a solution of the boundary-value problem (1)–(6).

Proceeding from the principle of iterative regularization [23], the unknown vector $\overline{p}$ can be determined through the minimization of the functional (10) by gradient methods of the first-order prior to the fulfilment of the condition:

$$J(\overline{p})\le\delta_f \tag{11}$$

where $\delta_f=\sum_{m=0}^{M}\int_{\tau_{\min}}^{\tau_{\max}}\sigma_m(\tau)\,d\tau$ is an integral error of the temperature measurements $f_m(\tau)$ and σ_m are the measurement variance.

To construct the iterative algorithm for this inverse problem, the solution of a conjugate gradient method is used. A successive approximation process is constructed as follows:

(i) *a-priori* an initial approximation of the unknown parameter vector $\overline{p}^0$ are set.

(ii) a value of the unknown vector at the next iteration are calculated as follows:

$$\begin{aligned}\overline{p}^{s+1}&=\overline{p}^{s}+\gamma^s\overline{g}^{s}\\ \overline{g}^{s}&=-\overline{J'}^{s}+\beta^s\overline{g}^{s-1}\end{aligned} \tag{12}$$

$$\beta^0 = 0, \beta^s = \left\langle \left(\overline{J_p'^{(s)}} - \overline{J_p'^{(s-1)}}\right), J_p'^{(s)} \right\rangle_{R^{N_p}} \Big/ \left\| J_p'^{(s)} \right\|_{R^{N_p}},$$

where $J_p'^{(s)}$ is the value of the functional gradient at the current iteration.

The alternative approach to estimating of ceramics properties can be found at [32–36].

3 RESULTS AND DISCUSSION

The evaluation of the linear coefficient of thermal expansion of C- and SiC-foam is reported in Fig. 6, the plot representing the CTE vs. temperature averaged on at least five specimens for each material type. A significant thermal stability can be assessed for both the tested foams over the whole temperature excursion. In particular, a fairly constant value just under 5×10^{-6}/°C is noticed for the SiC-foam, whereas the optimal performance provided by C-foam, which shows CTE values between 2–3 $\times$ 10^{-6}/°C, is affected at a range around 1000°C where the material suffers of a clear physical degradation. Lower density foams may swell when exposed to elevated temperatures because of gas expansion and increased pressure from inner cell air and moisture. If this happens, foam cells will then erupt and collapse since internal pressure is necessary to maintain cell structure: the contraction can continue until the foam becomes so dense that it resembles a solid more than a foamed

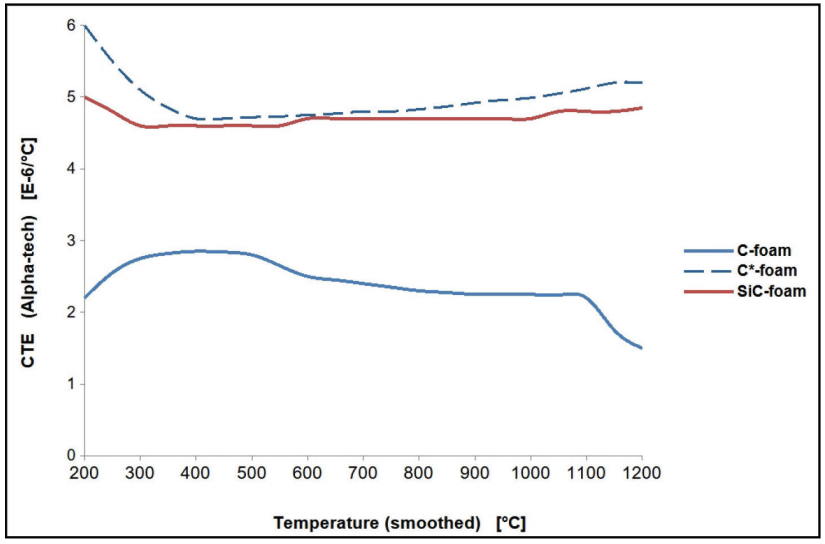

FIGURE 6
CTE evaluation of foam materials by linear dilatometer test.

plastic. Material stabilization may be obtained by prior annealing treatments, conditioning the as-received C-foam slab at 300–400°C for about 6–8 h, in order to remove inner lattice defects and residual stresses. As it is possible to see in the plot, the heat-treated carbon foam (C*-foam) maintains its structural stability at the highest temperature, but now the greater CTE values might induce heavier mechanical loads in the structure. Nevertheless, being the physical consistency an obvious requirement for the proposed ultra-high temperature space application, henceforward the carbon foam experimental results are referred to the annealed material.

The compression behavior of C- and SiC-foam is reported in Fig. 7, where the tensile stress (load) vs. strain (displacement) is given as average on at least five specimens for each material. The analysis of the load trend at initial strain and, mainly, the results obtained for the break load outline the different mechanical response provided by the two foams. Carbon foams don't crack when subjected to compression loads but they grind: this happen as the ligament strength is uniform along the surface of the sample. Silicon carbide foams crack when subjected to excessive compression loads, in fact they have a more rigid (less porous) structure respect to the carbon foams: thus, when the ligament starts to break the crack propagates into the sample. Definitely, a lower porosity results in the SiC-foam tougher-but-brittle behavior, whereas higher porosity allows C-foam to withstand loads by struts lattice effective buckling.

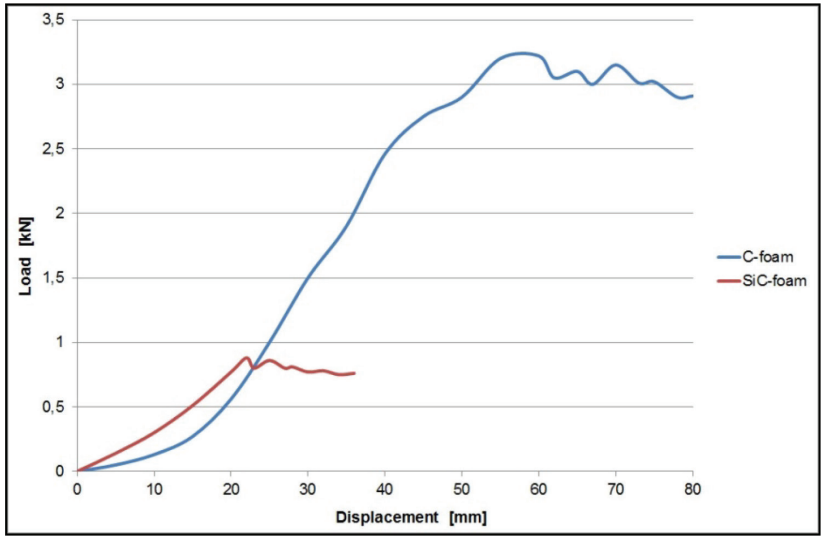

FIGURE 7
Mechanical properties of foam materials: tensile test.

The outgassing parameters of the foams tested in LSA-OTF were retrieved by sample/collector weight measurements, as summarized in Tab. 1; the reported values are obtained by averaging on the results of five specimens for each material, the uncertainties being taken as the higher between statistical deviation and blank test result (this latter representing the OTF actual sensitivity associated to each specific running test). Both the materials show TML <1% and CVCM <0.1%, thus they are fully compliant to the most adopted space mission requirements. However, it is possible to see that the C-foam tends to lose more matter by outgassing, which is probably due to a higher surface area (related to a greater level of open porosity) as well as to the absence of the protective SiC particles deposited on the foam carbon ligaments.

TABLE 1
Outgassing parameters of foam materials tested by OTF: M_{S0} (M_{C0}) and M_{S1} (M_{C1}) indicate the weight of samples (collectors) before and after the test, respectively, M_{S2} is the sample weight after moisture re-absorption.

	TML [%] $[(M_{S0} - M_{S1})/M_{S0}]$	**CVCM [%]** $[(M_{C1} - M_{C0})/M_{S0}]$	**RML [%]** $[(M_{S0} - M_{S2})/M_{S0}]$	**WVR [%]** [TML – RML]
C-foam	0.452 ± 0.022	0.018 ± 0.010	0.302 ± 0.008	0.150 ± 0.030
SiC-foam	0.202 ± 0.012	0.033 ± 0.007	0.133 ± 0.011	0.069 ± 0.023

The results of the evaluation of the two temperature-functions – thermal conductivity $\lambda(T)$ and volumetric heat capacity $C(T)$ – by inverse method solution are reported bellow. Detailed results of experiments are presented for SiC specimens (A – upper and B – lower). The weight and size of specimens and heat flux sensors are presented in the Table 2–3.

TABLE 2
The parameters of specimens.

Specimen	**Thickness, mm**	**Length, mm**	**Width, mm**	**Volume, cm^3**	**Weight, (before test), g**	**Density, kg/m^3**	**Weight, (after test), g**
A	25.80	100.95	74.00	192.73	121.90	0.632	120.10
B	25.60	100.25	74.20	190.43	108.02	0.567	105.20

TABLE 3
The parameters of heat flux sensors for specimens.

Sensors	**Thickness, mm**	**Length, mm**	**Width, mm**	**Volume, cm^3**	**Weight, (before test), g**	**Density, kg/m^3**
D_A	4.93	99.85	73.80	36.33	5.70	0.157
D_B	4.97	100.00	73.80	36.70	6.27	0.170

The thermocouples coordinates (measured from heating surfaces) are presented in Table 4.

TABLE 4
Coordinates of thermocouples.

Thermocouples	T_1	T_2	T_3	T_4	T_5	T_6
Coordinates, mm	12.90	25.80	30.73	12.80	25.60	30.53

The temperature measurements in specimens A and B are presented in Fig. 8.

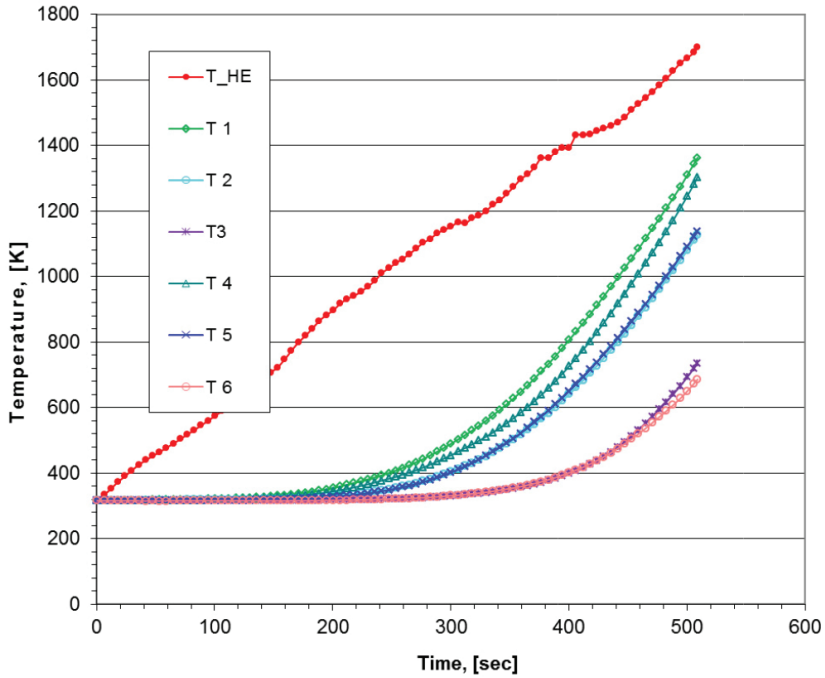

FIGURE 8
Temperature measurements (specimens A and B SiC).

Comparisons of the measured temperatures and calculated temperature (which was calculated using the thermal properties from inverse problems solving at the specimen A are presented in Fig. 9. Table 5 includes the obtained values of the least squares and the maximum deviation of the calculated temperatures from that measured in the experiments.

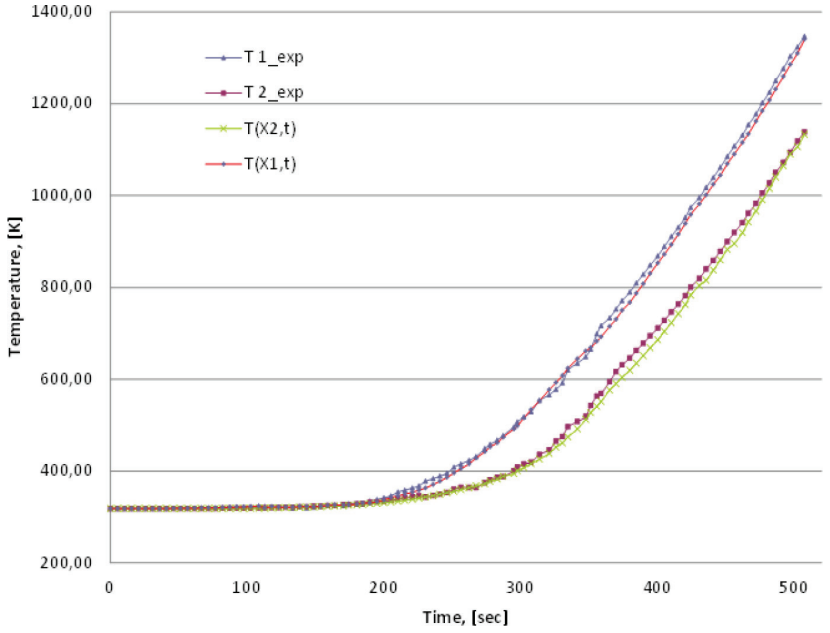

FIGURE 9
Comparison of the calculated in the thermocouples positions and measured temperatures of the specimen A.

TABLE 5
The deviation of the calculated temperatures.

Specimen	Least-squares temperature deviation, K	Maximum temperature deviation, K
A SiC	1.23	3.5
B SiC	1.13	3.9
A carbon foam	1.14	3.1
B carbon foam	1.21	3.6

The results of estimating the functions $C(T)$ and $\lambda(T)$ are presented in Fig. 10–11. Absolutely the same approach was used for estimating of thermal properties of carbon foam. The results of estimating of thermal properties of carbon foam also are presented in Fig. 10–11.

By observing the differential trend (i.e., at growing temperatures), it can be noticed that the more the foam increases its conductivity the less it is able to provide insulating capability. Comparing the two materials, it is possible to observe that SiC-foam conducts more than C-foam, also having better heat capacity, due to its higher density. Such result can be correlated to what found

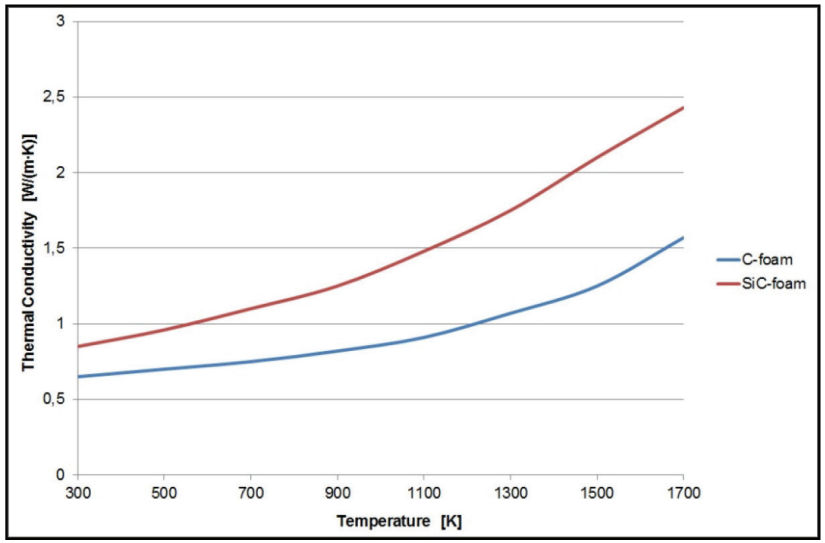

FIGURE 10
Estimated thermal conductivity of foam materials as function of temperature.

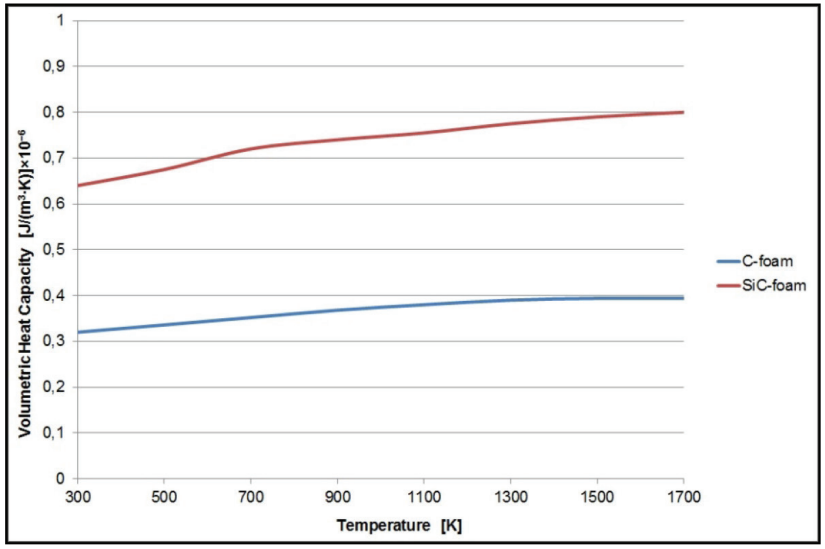

FIGURE 11
Estimated heat capacity of foam materials as function of temperature.

in CTE analysis: the struts dilatation can offer a wider path for heat conduction, as also suggested by the SiC-foam optical images taken before and after the harsh thermal conditioning (Fig. 12).

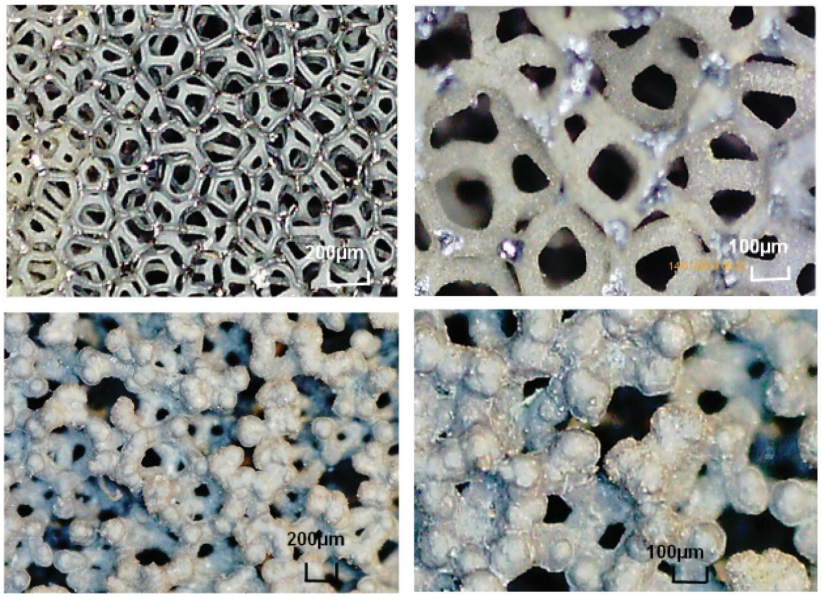

FIGURE 12
Optical micrographs of a SiC-foam sample surface before (top) and after (down) high temperature test.

The reported experimental results pointed out the potential benefits in adopting SiC-foam as sandwich core material for developing effective space TPS. In particular, a huge chemical stability under thermo-mechanical loads was demonstrated, including very stable behavior in terms of thermal expansion along the broad temperature excursion as well as a significant heat capacity at very high temperatures, thus ensuring the suite insulating properties for the required application. The comparison to the behavior shown by the pure carbon material establishes the noteworthy technical upgrade achievable by conceiving hybrid foams thanks to CVD method carried out to infiltrate and coat the bulk ligaments. It is revealed, in fact, that once the coating fills even just ~5% of the original pore space, the chemical and thermo-mechanical behavior of the whole is dominated by the properties of deposited material: in particular, when the coating is thick enough the foam physical response is virtually as if the carbon skeleton was absent and the deposition parameters can be controlled to improve and optimize the foam thermal properties. On the other hand, it has to be stressed that the use of C-foam might be advisable in operating conditions below over-critical temperatures (i.e., not beyond 1000°C), due to extreme lightness to thermal stability trade-off as well as to an established resilience to mechanical stress. In particular, it was demonstrated that the high porous carbon foam withstand significant compression loads without the structural breaking out occurring in more rigid and brittle

materials, thanks to a plastic-like deformation of the concave 3D array. Definitely, a thoughtful choice of foam typology for using in high-thermal applications (as for TPS sandwich core) should be strictly related to the specific mission operative parameters, in order to achieve the best solution balancing weight to temperature to mechanical load threshold constraints. Furthermore, it has to be mentioned that the present analysis is based on a uniform effective thermal conductivity approach, which might not be applicable near the surfaces of the layer of a porous thermal insulation, especially in the case of partially reflective neighboring materials. On this way, the reported findings aim to provide worth indications about carbon-based foams capabilities, with the objective to develop promising engineering solutions for a significant upgrade of the thermo-mechanical resistance of heat insulation systems and subsystems for spacecraft application.

4 CONCLUSIONS

Ceramic carbon-based foamed materials were characterized in terms of thermo-mechanical properties for ultra-high temperature space applications, such as for the core panel of sandwich-like structures designed as spacecraft thermal protection systems. Heat transport and insulating capability were investigated in details by experimental and numerical evaluation of thermal expansion, thermal conductivity and heat capacity as function of temperature in a wide range (300–1700°C); furthermore, compression tests were carried out as in-use loading of sandwich structures, while a thermo-vacuum characterization was performed in order to analyze the materials compliance to standard space environment operating requirements. The high porosity carbon foam showed significant thermal stability and resistance to combined thermo-mechanical stress, but cannot withstand extremely high temperature ranges (around and above 1000°C), which result detrimental for the material physical integrity. A prior foam annealing treatment may represent a solution to preserve the carbon foam bulk structure at highest temperatures, but at the expenses of optimal insulating performances. The hybrid silicon carbide foam demonstrated excellent thermo-mechanical stability, fully compliant outgassing behavior, and so high heat capacity to ensure the suite capability of heat flux containment for the proposed application, thanks to an effective refractory coating of the carbon bulk ligaments. As partial drawback, in this case the less porous material is heavier and, moreover, shows brittle behavior at exceeding tensile loads: its recommendation should be thus considered by paying close attention to the weight and mechanical resistance constraints of the specific space mission. By the way, the possibility of tuning the rate of silicon carbide coating of carbon inner structure sounds as effective route to achieve optimal thermal and mechanical properties by means of lightweight and multi-functional foams.

ACKNOWLEDGEMENTS

A part of this work, which was devoted to estimating of thermal properties of materials, was funded by the Russian Ministry of Science and Education in the frame of the Basic Research Project # FSFF-2020-0016.

REFERENCES

[1] Uyanna, O., Najafi, H. Thermal protection systems for space vehicles: A review on technology development, current challenges and future prospects, *Acta Astronaut.*, **176** (2020), 341, https://doi.org/10.1016/j.actaastro.2020.06.047

[2] Yang, Y.-Z., Yang, J.-L., Fang, D.-N. Research progress on thermal protection materials and structures of hypersonic vehicles, *Appl. Math. Mech.*, **29** (2008), 51, https://doi.org/10.1007/s10483-008-0107-1

[3] Shideler, J. L., Kelly, H. N., Avery, D. E. Multiwall TPS-an emerging concept, *J. Spacecraft Rockets*, **19** (1982), 7, https://doi.org/10.2514/3.62265

[4] Delfini, A., Santoni, F., Bisegna, F., Piergentili, F., Pastore, R., Vricella, A., Albano, M., Familiari, G., Battaglione, E., Matassa, R., Marchetti, M. Evaluation of atomic oxygen effects on nano-coated carbon-carbon structures for re-entry applications, *Acta Astronaut.*, **161** (2019), 276, https://doi.org/10.1016/j.actaastro.2019.05.048

[5] Wang, Y., Chen, Z., Yu, S., Awuye, D. E., Li, B., Liao, J., Luo, R. Improved sandwich structured ceramic matrix composites with excellent thermal insulation, *Compos. Part B-Eng.*, **129** (2017), 180, https://doi.org/10.1016/j.compositesb.2017.07.068

[6] Xu, Y., Xu, N., Zhang, W., Zhu, J. A multi-layer integrated thermal protection system with C/SiC composite and Ti alloy lattice sandwich, *Compos. Struct.*, **230** (2019), 111507, https://doi.org/10.1016/j.compstruct.2019.111507

[7] Gianchandani, P., Casalegno, V., Salvo, M., Bianchi, G., Ortona, A., Ferraris, M. SiC foam sandwich structures obtained by Mo-wrap joining, *Mater. Lett.*, **221** (2018), 240, https://doi.org/10.1016/j.matlet.2018.03.105

[8] Delfini, A., Albano, M., Vricella, A., Santoni, F., Rubini, G., Pastore, R., Marchetti, M. Advanced radar absorbing ceramic-based materials for multifunctional applications in space environment, *Materials*, **11** (2018), 1730, https://doi.org/10.3390/ma11091730

[9] Rawal, S. Materials and structures technology insertion into spacecraft systems: Successes and challenges, *Acta Astronaut.*, **146** (2018), 151, https://doi.org/10.1016/j.actaastro.2018.02.046

[10] Liang, C., Wang, Z., Wu, L., Zhang, X., Wang, H., Wang, Z. Light and strong hierarchical porous SiC foam for efficient electromagnetic interference shielding and thermal insulation at elevated temperatures, *ARC Appl. Mater. Interfaces*, **9** (2017), 23350, https://doi.org/10.1021/acsami.7b07735

[11] Albano, M., Micheli, D., Gradoni G., Bueno Morles, R., Marchetti, M., Moglie, F., Mariani Primiani, V. Electromagnetic shielding of thermal protection system for hypersonic vehicles, *Acta Astronaut.*, **87** (2013), 30, https://doi.org/10.1016/j.actaastro.2013.02.003

[12] Pastore, R., Delfini, A., Micheli, D., Vricella, A., Marchetti, M., Santoni, F., Piergentili, F. Carbon foam electromagnetic mm-wave absorption in reverberation chamber, *Carbon*, **144** (2019), 63, https://doi.org/10.1016/j.carbon.2018.12.026

[13] Colombi, P., Hellmann, J. Ceramic foams from preceramic polymers, *Mater. Res. Innov*., **6** (2002), 260, https://doi.org/10.1007/s10019-002-0209-z

[14] Manocha, S., Patel, K., Manocha, L. Development of carbon foam from phenolic resin via template route, *Indian J. Eng.Mater*. S., **17** (2010), 338, http://nopr.niscair.res.in/handle/123456789/10509

[15] Chen, C., Kennel, E. B., Stiller, A. H., Stansberry, P. G., Zondlo, J. W. Carbon foam derived from various precursors, *Carbon*, **44** (2006), 1535, https://doi.org/10.1016/j.carbon.2005.12.021

[16] Sarna, W., Kozakiewicz, J., Przybylski, J., Sylwestrazak, K. RVC-Reticulated vitreous carbon. Structure, precursor polymer materials, process of manufacturing and applications, *Inz. Mater*., **210** (2016), 81, https://DOI 10.15199/28.2016.2.6

[17] Harikrishnan, G., Umasankar Patro, T., Khakhar, D. V. Reticulated vitreous carbon from polyurethane foam–clay composites, *Carbon*, **45** (2007), 531, https://doi.org/10.1016/j.carbon.2006.10.019

[18] Fukushima, M., Colombo, P. Silicon carbide-based foams from direct blowing of polycarbosilane, *J. Europ. Ceram. Soc*., **32** (2012), 503, https://doi.org/10.1016/j.jeurceramsoc.2011.09.009

[19] Jana, P., Zera, E., Sorarù, G. D. Processing of preceramic polymer to low density silicon carbide foam, *Mater. Design*, **116** (2017), 278, https://doi.org/10.1016/j.matdes.2016.12.010

[20] Delfini, A., Pastore, R., Santoni, F., Piergentili, F., Albano, M., Alifanov, O. M., Budnik, S., Morzhukhina, A. V., Nenarokomov, A. V., Titov, D. M., Marchetti, M. Thermal analysis of advanced plate structures based on ceramic coating on carbon/carbon substrates for aerospace Re-Entry Re-Useable systems, *Acta Astronaut*., **183** (2021), 153, https://doi.org/10.1016/j.actaastro.2021.03.013

[21] Pastore, R., Delfini, A., Santoni, F., Marchetti, M., Albano, m., Piergentili F., Matassa, R. Space Environment Exposure Effects on Ceramic Coating for Thermal Protection Systems, *AIAA J. Spacecraft Rockets*, Published Online: 21 May 2021. https://doi.org/10.2514/1.A34997

[22] Pastore, R., Delfini, A., Albano, M., Vricella, A., Marchetti, M., Santoni, F., Piergentili, F. Outgassing effect in polymeric composites exposed to space environment thermal-vacuum conditions, *Acta Astronaut*., **170** (2020), 466, https://doi.org/10.1016/j.actaastro.2020.02.019

[23] Alifanov, O. M., Budnik, S. A., Nenarokomov, A. V., Michailov, V. V., Yudin, V. M. Identification of thermal properties of materials with applications for spacecraft structures, *Inverse Probl. Sci. En*., **12** (2004), 579, https://doi.org/10.1080/1068276042000219958

[24] Alifanov, O. M., Budnik, S. A., Mikhaylov, V. V., Nenarokomov, A. V., Titov, D. M., Yudin V. M. An experimental-computational system for materials thermal properties determination and its application for spacecraft structures testing, *Acta Astronaut.*, **61** (2007), 341, https://doi.org/10.1016/j.actaastro.2007.01.035

[25] Tseng, C. C., Sikorski, R. L., Viskanta, R., Chen, M. Y. Effect of foam properties on heat transfer in high temperature open-cell foam inserts, *J. Am. Ceram. Soc.*, **95** (2012), 2015, https://doi.org/10.1111/j.1551-2916.2012.05177.x

[26] Baillis, D., Coquard, R., Randrianalisoa, J. H., Dombrovsky, L. A., Viskanta, R. Thermal radiation properties of highly porous cellular foams, *Special Topics & Reviews in Porous Media*, **4** (2013), 111, https://doi.org/10.1615/SpecialTopicsRevPorousMedia.v4.i2.20

[27] Arduini-Schuster, M., Manara, J., Vo, C. Experimental characterization and theoretical modelling of the infrared-optical properties and the thermal conductivity of foams, *Int. J. Thermal Sci.*, **98** (2015), 156, https://doi.org/10.1016/j.ijthermalsci.2015.07.015

[28] Guevelou, S., Rousseau, B., Domingues, G., Vicente, J., Caliot, C., Flamant, G., Evolution of the homogenized volumetric radiative properties of a family of alfa-SiC foams with growing nominal pore diameter, *J. Porous Media*, **18** (2015), 1031, https://doi.org/10.1615/JPorMedia.2015012283

[29] Randrianalisoa, J., Baillis, D., Martin, C. L., Dendievel, R. Microstructure effect on thermal conductivity of open-cell foams generated from Laguerre–Voronoi tessellation method, *Int. J. Thermal Sci.*, **98** (2015), 277, https://doi.org/10.1016/j.ijthermalsci.2015.07.016

[30] Cunsolo, S., Coquard, R., Baillis, D., Bianco, N. Radiative properties modelling of open-cell solid foam: Review and new analytical law, *Int. J. Thermal Sci.*, **104** (2016), 122, https://doi.org/10.1016/j.ijthermalsci.2015.12.017

[31] Chai, Y., Yang, X. H., Zhao, M., Chen, Z. Y., Meng, X. Z., Jin, L. W., Zhang, Q. L., Hu, W. J. Study of microstructure-based effective thermal conductivity of graphite foam, ASME J. Heat Transfer, **139** (2017), 052004, https://doi.org/10.1115/1.4036002

[32] Y. Li, X.-L. Xia, C. Sun, S.-D. Zhang, and H. P. Tan, Integrated simulation of continuous-scale and discrete-scale radiative transfer in an open-cell foam made of semi-transparent absorbing-scattering ceramics, J. Quant. Spectr. Radiat. Transfer, **225** (2019), 156–165, https://doi.org/10.1016/j.jqsrt.2018.12.039

[33] Dugast, G., Settar, A., Chetehouna, K., Gascoin, N., De Bat, M. Experimental and numerical analysis on the thermal degradation of reinforced silicone-based composites: Effect of carbon fibres and silicon carbide powder contents, *Thermochim. Acta*, **686** (2020), 178563, https://doi.org/10.1016/j.tca.2020.178563

[34] Rong, Q., Wei, H., Huang, X., Bao, H. Predicting the effective thermal conductivity of composites from cross sections images using deep learning methods, *Compos. Sci. Tech.*, **184** (2019), 107861, https://doi.org/10.1016/j.compscitech.2019.107861

[35] Golyshev, V. D., Gonik, M. A., High-temperature thermophysical properties of nonscattering semitransparent materials II: determination of the thermal conductivity of melts in the presence of radiative – conductive heat transfer. High Temperatures – High Pressures. **24** (1992), 669–676.

[36] Chatillon, C., Bernard, C., Rocabois, P., High-temperature analysis of the thermal degradation of silicon-based materials. I: binary Si – O, Si – C, and Si – N compounds. High Temperatures – High Pressures. **31** (1999), 413–432.